

A microscopic investigation of the transition form factor in the region of collective multipole excitations of stable and unstable nuclei ¹

P. Papakonstantinou^{a,b}, E. Mavrommatis^b, J. Wambach^a, V.Yu. Ponomarev^{a,2}

^a*Institut für Kernphysik, Technische Universität Darmstadt, Schlossgartenstr.9,
D-64289 Darmstadt, Germany*

^b*Physics Department, Nuclear and Particle Physics Section, University of Athens,
GR-15771 Athens, Greece*

Abstract

We have used a self-consistent Skyrme-Hartree-Fock plus Continuum-RPA model to study the low-multipole response of stable and neutron/proton-rich Ni and Sn isotopes. We focus on the momentum-transfer dependence of the strength distribution, as it provides information on the structure of excited nuclear states and in particular on the variations of the transition form factor (TFF) with the energy. Our results show, among other things, that the TFF may show significant energy dependence in the region of the isoscalar giant monopole resonance and that the TFF corresponding to the threshold strength in the case of neutron-rich nuclei is different compared to the one corresponding to the respective giant resonance. Perspectives are given for more detailed future investigations.

PACS: 21.60.Jz; 21.10.Re; 24.30.Cz

1 Introduction

The multipole response of nuclei at energies below the quasielastic regime is characterized by various collective excitations. Among these, giant resonances (GRs) of stable nuclei have been investigated for decades, both theoretically and experimentally [1, 2, 3]. Macroscopically, they are interpreted as small-amplitude excitations corresponding to the propagation of zero sound in the nuclear medium. Collective modes of excitation at energies below GRs include surface vibrations and rotations of the nuclear body. Transverse modes of excitation, corresponding to oscillations of the current distribution, also exist - a well-known example being the twist mode [4] and perhaps the toroidal mode [5]. At energies higher than GRs, overtones of GRs are examined [6, 7, 8, 9]. Despite the long-time effort devoted to the understanding of nuclear collective motion, several issues remain open; as far as the electric response of spherical stable nuclei is concerned, we may mention as examples the fine structure of GRs, the experimental energy-weighted sum rule (EWSR) of compression modes (isoscalar monopole and dipole resonances), the relation between the energy of the latter and the value of nuclear matter incompressibility, the identification of isovector quadrupole GRs and the nature of low-lying collective modes [2, 3].

Nowadays, it is feasible in addition to study experimentally the properties of unstable nuclei, in radioactive ion beam facilities. Access to their multipole response appears possible using inverse kinematics or double storage rings. The physics of nuclei far from stability is rich in new phenomena, owing to the presence of very weakly bound nucleons, the unusual ratio N/Z (for given mass number) and the large difference between the proton and neutron Fermi energies. The structure of the particle continuum

¹Work supported in part by Deutsche Forschungsgemeinschaft within the SFB 634 and by the University of Athens under grant 70/4/3309.

²Permanent address: JINR, Dubna, Russia.

and the nature of low-lying strength in unstable nuclei is of particular importance, as they provide information on decay properties, polarizabilities, shell structure etc. At present, limited experimental information is available. The giant dipole resonance of neutron-rich Oxygen isotopes has been under study, as well as the dipole response of various light unstable nuclei (eg. neutron-rich He, Li, Be, C isotopes and proton-rich ^8Be and ^{13}O) [10]. Information is available on the low-lying quadrupole strength of various unstable nuclei [11]. Theory has been anticipating experiment to some extent, and has by now provided interesting predictions regarding the low-energy response and GRs of nuclei far from stability. For example, a considerable mixing of isoscalar and isovector transitions and an increased fragmentation of GRs are expected. A special feature of the response of very neutron-rich nuclei is the so-called threshold strength, namely the significant amount of isoscalar and non-collective strength predicted to occur just above the neutron threshold. In the case of open-shell nuclei, the shell model [12] and the Quasiparticle RPA (QRPA) [13, 14, 15, 16] have been applied. Relativistic RPA (RRPA) has been used as well [17, 18]. Results on doubly magic nuclei have been obtained with standard RPA (with or without inclusion of higher-order configurations) or Continuum RPA (CRPA) methods; in particular, the self-consistent Skyrme-Hartree-Fock + Continuum RPA (SHF+CRPA) has been used for a systematic study of the response of nuclei far from stability by the group of I. Hamamoto [19, 20, 21, 22, 23] and recently by our group [24, 25]. For more information on the relevant theoretical and experimental activity, one can refer, for example, to the contributions in Ref. [3].

The RPA method describes satisfactorily the transition densities of collective states in stable nuclei. In the past the RPA has also been used to study transition densities and currents of individual excitations in the case of unstable nuclei and to compare with the behaviour of stable nuclei [19, 20, 21, 22, 23, 24, 25, 26, 27, 28]. In this work we focus on the transition densities and form factors corresponding to electric excitations of stable and unstable nuclei, adopting an approach which allows a systematic study. Using the SHF+CRPA method, we will examine how the transition strength distribution of selected Sn and Ni isotopes, and for low multipolarities, varies with the momentum q transferred to the system. For this we will consider an external field of the form $j_L(qr)$. The momentum dependence of the nuclear response can be studied experimentally using inelastic electron scattering. Further information accessible in inelastic electron scattering experiments concerns the transition current density, which has been the subject of a separate work [25].

The purpose of the present pursuit is twofold. First of all, it is important to have a reliable microscopic description of the transition density characterizing a nuclear excitation - either of a stable or an unstable nucleus - not only to gain insight into the nature of the excitation, but also because theoretical transition densities enter the analysis of electron- or hadron-scattering experiments aiming at identifying GRs. Theoretically, the transition density associated with a particular type of excitation approaches hydrodynamical behaviour in the case of very collective states, such as GRs, but in general it is expected to be energy dependent. Therefore, macroscopic descriptions may be inadequate in certain cases. Our approach will help us to pinpoint cases where the transition density varies significantly with excitation energy. Possible candidates are resonances with large fragmentation width. Second, we wish to contribute to the theoretical understanding, currently being formed, of the response of unstable nuclei, as a guidance to future experimental activity. Inevitably, some of the results obtained using conventional models and interaction parametrizations (fitted to describe the properties of stable nuclei) will be proven inaccurate by the future experimental research, but there is much to be learned in the process.

In Sec. 2 the quantities of interest are defined and our method of calculation is presented. Results for spherical, closed-shell Sn and Ni isotopes are presented and

discussed in Sec. 3. Conclusions and perspectives are given in Sec. 4.

2 Definitions and method of calculation

We consider the response of spherical, closed-(sub)shell nuclei to an external field of the type

$$V = \sum_{i=1}^A V_L(r_i, \tau_i) Y_{L0}(\theta_i, \phi_i),$$

where the variable $\tau_i = p$ or n labels the isospin character -proton or neutron- of the i -th particle. For an isoscalar (IS) field, $V_L(r, p) = V_L(r, n) \equiv V_L(r)$ and for an isovector (IV) one $V_L(r, p) = -V_L(r, n) \equiv V_L(r)$. For $L = 1$ we use an effective charge equal to $-\frac{N}{A}$ for protons and $\frac{Z}{A}$ for neutrons. In the following, the isospin label will be suppressed for the sake of simplicity.

We set

$$V_L(r) = [4\pi(2L+1)]^{1/2} j_L(qr),$$

where j_L is a spherical Bessel function. In the long-wavelength limit $qR \rightarrow 0$ (R is the nuclear radius), we obtain the usual multipole operator of the form r^K , where $K = L$ for $L > 0$ and $K = 2$ for $L = 0$. The transition density $\delta\rho_{L0}(\vec{r}, E)$, characterizing the excited natural-parity state $|L0\rangle$ of energy E , is determined by its radial component $\delta\rho_L(r, E)$, where

$$\delta\rho_{L0}(\vec{r}, E) = (2L+1)^{-1/2} \delta\rho_L(r, E) Y_{L0}(\theta, \phi) / r^2. \quad (1)$$

For IS (IV) transitions, this is the sum (difference) of the proton- and neutron-transition densities. The strength distribution

$$S(E, q) = \sum_f |\langle 0|V|f\rangle|^2 \delta(E - E_f)$$

(where $|f\rangle$ are the final states, excited by the q -dependent external field V and E_f their excitation energies) is related to the transition form factor $F_L(q^2, E)$, i.e. to the Fourier transform of $\delta\rho_{L0}(\vec{r}, E)$. In particular, since we are dealing with continuous distributions, we write the strength in a small energy interval of width ΔE at energy E as

$$\begin{aligned} S(E, q) &= \frac{4\pi(2L+1)}{\Delta E} \left| \int_0^\infty dr \delta\rho_L(r, E) j_L(qr) \right|^2 \\ &= \frac{(2L+1)}{\Delta E} \left| \int d^3r \delta\rho_{L0}(\vec{r}, E) e^{i\vec{q}\cdot\vec{r}} \right|^2 \propto |F_L(q^2, E)|^2. \end{aligned} \quad (2)$$

As long as charge-current conservation is respected, the calculated $S(E, q)$ may be interpreted as the longitudinal response function entering the analysis of inelastic electron scattering within the Born approximation [29].

Our aim is to search for variations of the transition density in the region of collective excitations. By looking at the strength distribution $S(E, q)$ corresponding to different values of momentum q , we will “probe” the various momentum- (Fourier-) components of $\delta\rho_L$, according to Eq. (2). In a scenario where the $\delta\rho_L$ (and F_L) turns out to be the same, within a proportionality factor $f(E)$, for all transitions making up a strength distribution $S(E, q)$, the shape of the calculated $S(E, q)$, determined by $f^2(E)$, should not change with q . In realistic cases there will be non-trivial variations of the $\delta\rho_L$ with the energy, revealing the different microscopic structure of the various transitions.

Following the standard RPA method, we consider particle-hole (ph) excitations, built on top of the Hartree-Fock (HF) nuclear ground state and subjected to the ph residual interaction (HF+RPA method). In particular, the quantities introduced above are calculated using a Skyrme - Hartree-Fock (SHF) plus Continuum - RPA (CRPA) model. For the HF ground-state, the numerical code of P.-G. Reinhard [30] is used. The calculation of the response function (unperturbed HF, as well as RPA) is formulated in coordinate space, as described in [31, 32, 33, 34, 35]. The radial part of the unperturbed ph Green function, of multipolarity L and specified isospin character, is given by:

$$G_L^0(r, r'; E) = \sum_{ph} \left\{ \frac{\langle p || O_L || h \rangle_r^* \langle p || O'_L || h \rangle_{r'}}{\varepsilon_{ph} - E} \pm \frac{\langle h || O'_L || p \rangle_{r'}^* \langle h || O_L || p \rangle_r}{\varepsilon_{ph} + E} \right\}, \quad (3)$$

where O_L (or O'_L) is one of the operators Y_L , $[Y_L \otimes (\nabla^2 + \nabla'^2)]_L$, $[Y_{L\pm 1} \otimes (\vec{\nabla} - \vec{\nabla}')]_L$ and $[Y_{L\pm 1} \otimes (\vec{\nabla} + \vec{\nabla}')]_L$. The sign of the second term depends on the symmetry properties of the operators O_L and O'_L under parity and time-reversal transformations. Spin operators have been omitted in the present calculation. With h (p) we denote the quantum numbers of the HF hole (particle) state and $\varepsilon_{ph} = \varepsilon_p - \varepsilon_h$ is the energy of the unperturbed ph excitation. The particle continuum is fully taken into account, as described in [31, 34, 36]. A small but finite $\text{Im}E$ ensures that bound transitions acquire a finite width [31].

The RPA ph Green function is given by the equation

$$G_L^{\text{RPA}} = [1 + G_L^0 V_{\text{res}}]^{-1} G_L^0, \quad (4)$$

which is solved as a matrix equation in coordinate space, isospin character and operators O_L . The ph residual interaction V_{res} is zero-range, of the Skyrme type, derived self-consistently from the Skyrme-HF energy functional [34, 37]. From the Green function G_L^{RPA} for $O_L = O'_L = Y_L$ the strength distribution $S(E, q)$ is obtained as

$$S(E, q) = 4(2L + 1) \text{Im} \int j_L(qr) G_L^{\text{RPA}}(r, r'; E) j_L(qr') dr dr'. \quad (5)$$

Within the RPA, giant resonances (GRs) are generated as coherent ph excitations between major $n\ell$ shells; for example, $\Delta N=2$ for the giant monopole and quadrupole resonances (GMR and GQR) and $\Delta N=1$ for the isovector (IV) giant dipole resonance (GDR), where $N = 2n + \ell$ is the energy quantum number of a shell. Therefore, a GR lies energetically in the neighbourhood of the $\Delta N \hbar \omega$ region, where the energy quantum $\hbar \omega \approx 41A^{-1/3}$ MeV, within the simple harmonic-oscillator model. Its precise position relative to this value (lower or higher) is determined by the ph residual interaction (attractive or repulsive). ‘‘Overtones’’ of GRs are generated as $\Delta N' = \Delta N + 2$ excitations. An example is the isoscalar (IS) GDR, which lies energetically in the $3\hbar \omega$ region. The HF+RPA method can also describe low-lying transitions with $\Delta N=0$ (2^+ , 4^+ etc), provided that the nucleus considered is not $n\ell$ -closed.

3 Results and discussion

We have applied our method to six cases of spherical, closed-shell nuclei lying inside, close to or far away from the valley of stability. In particular, we have examined the isotopes $^{56,78,110}\text{Ni}$ and $^{100,120,132}\text{Sn}$. ^{56}Ni is the next heavier $Z = N$, doubly closed nucleus after ^{40}Ca . It is β -unstable, but lies very close to the stability line; being closed-shell, ^{56}Ni is the most stable Ni isotope where our model could be applied, since pairing is not included in the model. ^{78}Ni is a neutron-rich isotope, possibly doubly magic [38]. As was done before in Refs. [19, 25], we have used the extremely neutron-rich

configuration ^{110}Ni as an academic example of a closed-shell isotope in the vicinity of the neutron drip line. According to SHF results, the $N = 82$ closure may still be valid in the Ni region [19], although not conclusively. Lying on the proton-rich side of the nuclear chart and with a half life of the order of 1s [39, 40], ^{100}Sn may be the heaviest $N = Z$ nucleus inside the proton drip line. ^{120}Sn is a stable, doubly magic Sn isotope, while ^{132}Sn is a neutron-rich isotope with a half-life of 39.7s [41] and among the most magic heavy nuclei, as no excited states of this nucleus have been detected below 4 MeV [42].

We have calculated the IS and IV monopole (ISM and IVM), IV dipole (IVD) and IS and IV quadrupole (ISQ and IVQ) response of the nuclei $^{56,78,110}\text{Ni}$ and $^{110,120,132}\text{Sn}$ using the RPA method described in the previous section, for $q = 0.2, 0.4, 0.6, 0.8, 1.0 \text{ fm}^{-1}$. We have employed the Skyrme parametrization SkM*[43], tailored to describe GRs of stable nuclei and used in previous studies of the response of exotic nuclei as well, eg. in Refs. [19, 20, 21, 22, 23, 24, 25, 26, 27]. We have also used the Skyrme force MSk7 [44], whose parameters were determined by fitting the values of nuclear masses, calculated using the HF+BCS method, to the measured ones, for 1888 nuclei with various values of $|N - Z|/A$. The two forces have similar nuclear-matter properties, except for the effective mass m^* . The results obtained with the two Skyrme parametrizations agree qualitatively. Therefore, we only show results obtained with SkM*.

Selected results are presented in Figs. 1-5. In Figs. 6-8 the radial part of the proton- and neutron- transition density is plotted for some cases. We notice that, in all examined cases, as q increases, the strength distribution is shifted to higher energies, which can be interpreted as the onset of the quasielastic peak. The continuum becomes increasingly important. Also, overtones of giant resonances become visible. For instance, in the ISM response, Fig. 1, strength is shifted from the $2\hbar\omega$ region (the IS GMR) to the $4\hbar\omega$ region. In the IVD response, Fig. 4, strength is found in the $3\hbar\omega$ region as q increases. Excitations of single-particle character, with density oscillations taking place in the interior of the nucleus, give rise to this behaviour of the form factor - cf., for example, Fig. 8, right panel, where the IVM transition density of ^{132}Sn at 46 MeV is shown. In the medium-heavy nucleus ^{56}Ni the shift takes place more slowly as a function of q than in heavier nuclei, such as ^{120}Sn , because a narrower density distribution corresponds to a broader form factor.

Next we discuss our results in more detail.

3.1 Isoscalar monopole response and compression modes

In Fig. 1 the ISM response of ^{56}Ni , ^{110}Ni and ^{120}Sn is presented. Observing the values of the strength distribution of ^{120}Sn for the various values of q , we notice that the form factor of the weak peaks on the high-energy tail of the GMR has a weaker q -dependence, between $q = 0.4 - 0.8 \text{ fm}^{-1}$, compared to the GMR peak. The same holds for the other Sn isotopes and for ^{78}Ni (not shown). The GMR width of the medium-heavy nucleus ^{56}Ni is large, compared to the GMR width of heavier nuclei. In Fig. 1 (left panel) two distinct energy regions can be recognized in the ISM strength distribution of ^{56}Ni : the region $P_<$ below $\mathcal{E}_0 \approx 23 \text{ MeV}$, and the region $P_>$ above \mathcal{E}_0 . According to macroscopic models, the GMR is a uniform compression mode whose transition density has a node at the nuclear surface. The node would then occur at radius $R \approx 1.2A^{1/3} = 4.6 \text{ fm}$ (or 4.3 fm, if we use our SHF result for the radius) in ^{56}Ni . Therefore, the transition density would show maximal overlap with the function $j_0(qr)$ (whose 1st root equals π) for $q = q_{01} = \pi/R = 0.68$ (or 0.73) fm^{-1} . It seems that the form factor in the region $P_<$ follows, at least approximately, this type of behaviour, since it reaches a maximum between 0.6 and 0.8 fm^{-1} . The form factor in $P_>$ is maximized at a larger value of q and therefore it does not correspond to such a picture. Indeed, as we observe in Fig. 6, the transition density in the regime $P_>$ has a node at a smaller radius than in $P_<$, by

about 0.5 fm, and one more node at a larger radius.

The fragmentation of the GMR is a typical feature of light and medium-heavy nuclei. It seems therefore important, for an accurate evaluation of the EWSR and the centroid energy of the GMR in those nuclei, to take into account the energy dependence of the transition density in the analysis of the relevant α -scattering experiments - see also the analysis in Ref. [45]. The same may hold for the IS giant dipole resonance (GDR), which, in addition, appears to have large width even for nuclei as heavy as ^{208}Pb . Moreover, the amount and nature of the strength detected below the main IS GDR peak (which is located at approximately 23 MeV for heavy nuclei) has not been clarified. For a recent report on the issue - see eg. the contribution of U. Garg in Ref. [3]. Given that the properties of the IS GMR and GDR are used for determining the value of nuclear matter incompressibility, a detailed examination may be recommended. We have not presented calculations of the IS GDR here, as our method lacks full self-consistency (due to the omission of spin-dependent terms from the residual interaction) and therefore our results would not be free of spurious components.

3.2 Isoscalar quadrupole response

The two peaks in the ISQ strength distribution of the nuclei considered here are the low-lying collective 2^+ transition (first peak) and the IS GQR (second peak). In the cases of ^{56}Ni (see Fig. 2), ^{78}Ni (not shown) and $^{100,120}\text{Sn}$ (not shown), the two peaks show similar behaviour as a function of q up to $q \approx 0.8 \text{ fm}^{-1}$. This is due to the fact that in these nuclei, the transition density of both states is peaked close to the surface. It should be noted, however, that the nature of the two peaks may be quite different, as the low-lying state is expected to be characterized by non-negligible vorticity [24, 25]. We also find that the transition density corresponding to the low-lying state has a node inside the nucleus. In the case of ^{132}Sn (Fig. 2), the form factor of the first peak does not follow the behaviour of the GQR form factor. In ^{110}Ni (Fig. 2), there is a clear difference. The low-energy peak loses its strength faster than the GQR, as q increases, behaving like the threshold strength of other multiplicities - which we discuss in § 3.4. Respective transition densities are plotted in Fig. 7. In ^{110}Ni , a third peak occurs between the low-lying state and the GQR, also showing different behaviour. Its strength peaks at higher q than the GQR and the low-lying-state strength. It is a non-collective state with a transition density localized in the interior of the nucleus. Such a peak occurs also in the case of ^{78}Ni (not shown) and ^{132}Sn . Corresponding transition densities are also plotted in Fig. 7. They indicate that these secondary peaks are not of pure IS character.

The experimental width and fragmentation of the IS GQR can be much larger than accounted for by first-order RPA calculations. In order to reproduce the experimental width of the GQR one has to take into account higher-order configurations than $1p1h$ [46, 47]. Then one would be in a position to examine the energy dependence of the transition density in the region of the GQR.

3.3 Isovector strength distributions

As shown in Fig. 3, the IVM response of neutron-rich nuclei is dominated by two structures, namely the broad peak of the IV GMR above 25 MeV, higher than the IS GMR due to the repulsive IV residual interaction, and an amount of strength at the IS GMR region. The latter is of IS character (see Fig. 8, left panel) and exemplifies the admixture between IS and IV transitions in neutron-rich nuclei. A similar situation is observed in the IVQ response (Fig. 5); most of the IVQ strength, making up the IV GQR, lies above 20 MeV, but an amount of strength remains in the IS GQR region. In all nuclei, the IV GMR and GQR have a width of several MeV.

No significant energy dependence of the transition density is observed in the region of the IV GMR and GQR for the low values of q examined here. With the exception of the threshold strength in very-neutron-rich nuclei (see § 3.4), the IVM strength distributions in Fig. 3 for $q = 0.2, 0.4$ and 0.6 fm^{-1} are similar to each other. The same seems to hold for the IVQ distributions (Fig. 5), in the region of the IV GQR, in spite of the rich fine structure of the latter. In the case of the IVD distributions in Fig. 4 this holds to a lesser extent.

The nature and systematics of the low-lying dipole strength is of particular importance in connection to astrophysical processes. A detailed examination of the IV as well as IS dipole strength distribution and also the corresponding vorticity strength distribution for various nuclei, including the momentum dependence of these distributions, using a fully self-consistent method, should be able to clarify - from a theoretical point of view - important issues such as the admixture of IS and IV transitions at low energies, the existence of toroidal modes and the energy dependence of the transition densities and currents in the region of the IS GDR.

3.4 Threshold strength

As mentioned in the introduction, the response of very neutron-rich nuclei is characterized by the so-called threshold strength [19, 20, 22, 23, 27]. The effect is expected when the neutron threshold lies much lower than the GR region - which begins typically at about 10 MeV. The values of the particle threshold energy E_t for the isotopes $^{56,78,110}\text{Ni}$ and $^{100,120,132}\text{Sn}$ and for the multipolarities considered here are presented in Fig. 9. According to our results, the threshold strength vanishes as q increases. This is seen clearly in the case of ^{110}Ni . As we observe in Fig. 1 (middle panel), the ISM threshold strength, appearing as a “shoulder” at low energy, behaves differently than the peak at around 13.5 MeV; thus we have a way to discriminate between the “threshold strength” and the main peak - which represents the GMR. The same holds for the IVM response of ^{132}Sn (see Fig. 3, right panel) and similarly for the IVD (see Fig. 4, middle panel). The distribution of loosely bound neutrons at large distances from the nuclear center results in form factors F_L with maxima at low values of q , giving rise to this type of behaviour of the threshold strength. The effect of the excess neutrons and the origin of the threshold strength is demonstrated in Figs. 6 (^{110}Ni , compare right-top panel with the other panels) and 8 (^{132}Sn , left panel), where typical examples of transition densities corresponding to the threshold region are presented.

In Ref. [22] the ISM response of the neutron-rich nucleus ^{60}Ca is examined - where a significant amount of threshold strength appears as well. It was found that in the region of the GMR the transition density compares rather well with the Tassie model prediction, whereas in the threshold region it is extended at large distances and it originates mostly from neutron excitations. A similar effect was predicted also in the case of the ISQ response of ^{28}O [20]. Our results are in concordance with these findings.

4 Conclusion and perspectives

In this work we have used the SHF+CRPA method to study the low-multipolarity response of selected Ni and Sn isotopes and to examine in particular variations of the transition density and form factor in the region of collective excitations. According to our results, the transition density may show considerable energy dependence in the region of the IS GMR. This should be taken into account in the analysis of relevant hadron scattering experiments. The form factor, corresponding to the threshold strength in very-neutron-rich nuclei, is narrower compared to the form factor of the respective

giant resonance. This result, owing to the loosely bound neutrons outside the core, is independent of L . In the region of IV GMR and GQR resonances, no significant energy dependence is observed for q values below 1.0 fm^{-1} . A detailed examination of the IS and IV dipole strength distribution, as well as the corresponding vorticity strength distribution, should be the subject of future work. Special care should be taken of the spurious center-of-mass motion. Important issues to be addressed include the admixture of IS and IV transitions at low energies, the existence of toroidal modes and the energy dependence of the transition densities and currents in the region of the IS GDR.

References

- [1] “Electric and Magnetic Giant Resonances in Nuclei”, Ed. Speth J, World Scientific 1991.
- [2] Proc. Int. Conf. on Giant Resonances, Osaka, June 12-15 2000, *Nucl. Phys. A* **687** (2001).
- [3] Proc. COMEX1, Int. Conf. on Collective Motion under Extreme Conditions, Paris, June 10-13 2003, *Nucl. Phys. A* **731** (2004).
- [4] Vinas X et al 2001, *Phys. Rev. A* **64** 055601; Reitz B et al 2002, *Phys. Lett. B* **532** 179.
- [5] Ryezayeva N et al 2002, *Phys. Rev. Lett.* **89** 272502.
- [6] Shlomo S and Sanzhur A I 2002, *Phys. Rev. C* **65** 044310.
- [7] Shlomo S, Kolomietz V M and Agrawal B K 2003, *Phys. Rev. C* **68** 064301.
- [8] Gorelik M L and Urin M H 2001, *Phys. Rev. C* **64** 047301.
- [9] Clark H L, Lui Y-W and Youngblood D H 2001, *Phys. Rev. C* **63** 031301(R).
- [10] Aumann T et al 2001, *Nucl. Phys. A* **687** 103c and Refs. therein.
- [11] Raman S, Nestor C W and Tikkanen P 2001, *At. Data Nucl. Data Tables* **78** 1.
- [12] Sagawa H 2002, *Eur. Phys. J. A* **13** 87.
- [13] Khan E and Van Giai N 2000, *Phys. Lett. B* **66** 472.
- [14] Colo G and Bortignon P F 2001, *Nucl. Phys. A* **696** 427.
- [15] Matsuo M 2001, *Nucl. Phys. A* **696** 371.
- [16] Khan E, Sandulescu N, Grasso M and Van Giai N 2002, *Phys. Rev. C* **66** 024309.
- [17] Vretenar D, Paar N, Ring P and Lalazissis G A 2001, *Nucl. Phys. A* **692** 496.
- [18] Vretenar D, Paar N, Ring P and Niksic T 2002, *Phys. Rev. C* **65** 021301(R).
- [19] Hamamoto I, Sagawa H and Zhang X Z 1996 *Phys. Rev. C* **53** 765.
- [20] Hamamoto I and Sagawa H 1996 *Phys. Rev. C* **54** 2369.
- [21] Hamamoto I, Sagawa H and Zhang X Z 1997 *Phys. Rev. C* **55** 2361.
- [22] Hamamoto I, Sagawa H and Zhang X Z 1997 *Phys. Rev. C* **56** 3121.

- [23] Hamamoto I, Sagawa H and Zhang X Z 1999 *Nucl. Phys. A* **648** 203.
- [24] Papakonstantinou P 2004, PhD Thesis, University of Athens.
- [25] Papakonstantinou P, Wambach J, Mavrommatis E and Ponomarev V Yu 2004 *Phys. Lett. B* **604** 157.
- [26] Catara F, Lanza E G, Nagarajan M A and Vitturi A 1997 *Nucl. Phys. A* **614** 86.
- [27] Catara F, Lanza E G, Nagarajan M A and Vitturi A 1997 *Nucl. Phys. A* **624** 449.
- [28] Kamedzhiev S, Speth J and Tertychny G 1997, *Nucl. Phys. A* **624** 328.
- [29] Ciofi degli Atti C 1980, *Prog. Part. Nucl. Phys.* **3** 163.
- [30] Reinhard P-G 1991, “Skyrme-Hartree-Fock Model” in *Computational Nuclear Physics I - Nuclear Structure*, ed. Langanke K, Maruhn J E and Koonin S E (Springer, New York) p.28.
- [31] Bertsch G 1991, “The Random Phase Approximation for Collective Excitations”, *ibid* p.75.
- [32] Bertsch G F and Tsai S F 1975, *Phys. Rep.* **18C** 127.
- [33] Van Giai N and Sagawa H 1981, *Nucl. Phys. A* **371** 1.
- [34] Nguyen Van Giai 1983 in *Nuclear Collective Dynamics* (World Scientific) p.356.
- [35] Ryckebusch J, Waroquier M, Heyde K, Moreau J and Ryckbosch D 1988 *Nucl. Phys. A* **476** 237.
- [36] Shlomo S and Bertsch G F 1975, *Nucl. Phys. A* **243** 507.
- [37] Tsai S F 1978, *Phys. Rev. C* **17** 1862.
- [38] Daugas J M et al. 2000 *Phys. Lett. B* **476** 213.
- [39] Schneider R et al 1994, *Z. Phys. A* **348** 241;
- [40] Faestermann T et al. 1995, GSI Annual Report, p. 23.
- [41] Audi G, Bersillon O, Blachot J and Wapstra A H 2003, *Nucl. Phys. A* **729** 3.
- [42] Bhattacharyya P et al. 2001 *Phys. Rev. Lett.* **87** 062502.
- [43] Bartel J, Quentin P, Brack M, Guet C and Hakansson H-B 1982 *Nucl. Phys. A* **386** 79.
- [44] Goriely S, Tondeur F and Pearson J M 2001, *At. Data Nucl. Data Tables* **77** 311.
- [45] Kamedzhiev S, Speth J and Tertychny G 2000 *Eur. Phys. J. A* **7** 483.
- [46] Drożdż S, Nishizaki S, Speth J and Wambach J 1990, *Phys. Rep.* **197** 1.
- [47] Speth J and Wambach J 1991, “Theory of Giant Resonances” in [1], p.1.

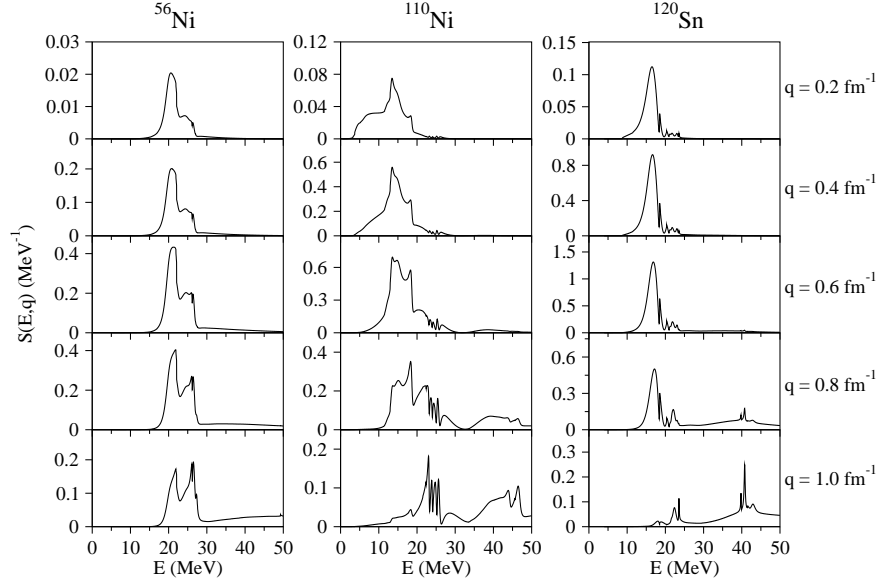


Figure 1: ISM strength distribution as a function of energy and momentum transfer.

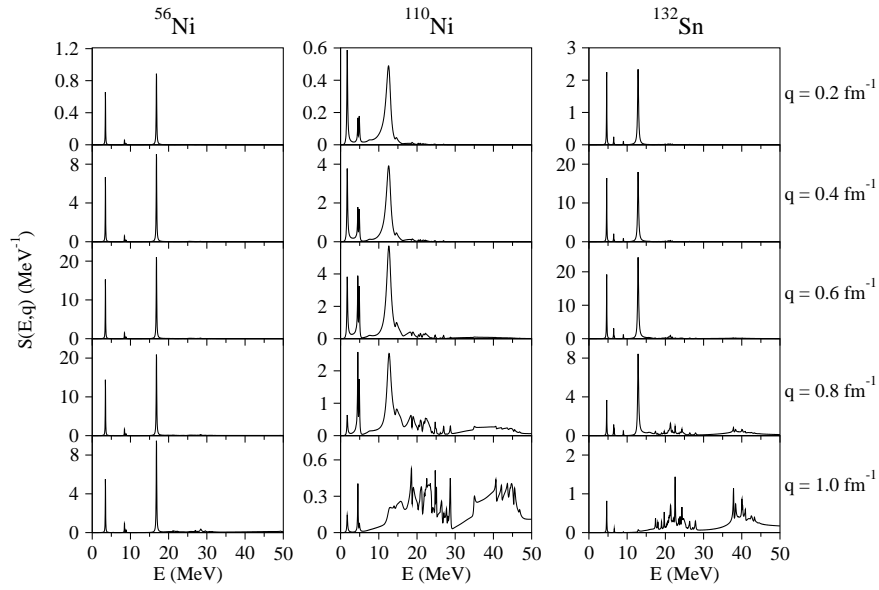


Figure 2: ISQ strength distribution as a function of energy and momentum transfer.

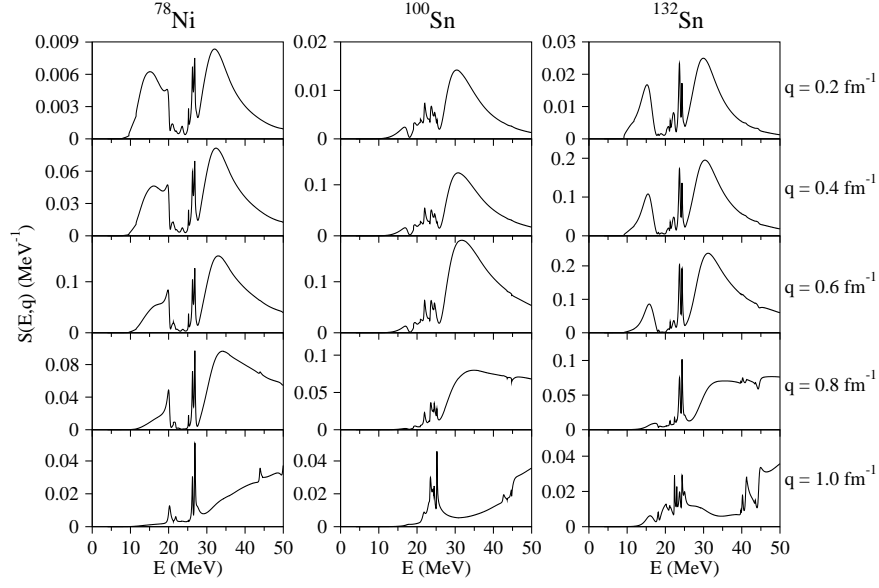


Figure 3: IVM strength distribution as a function of energy and momentum transfer.

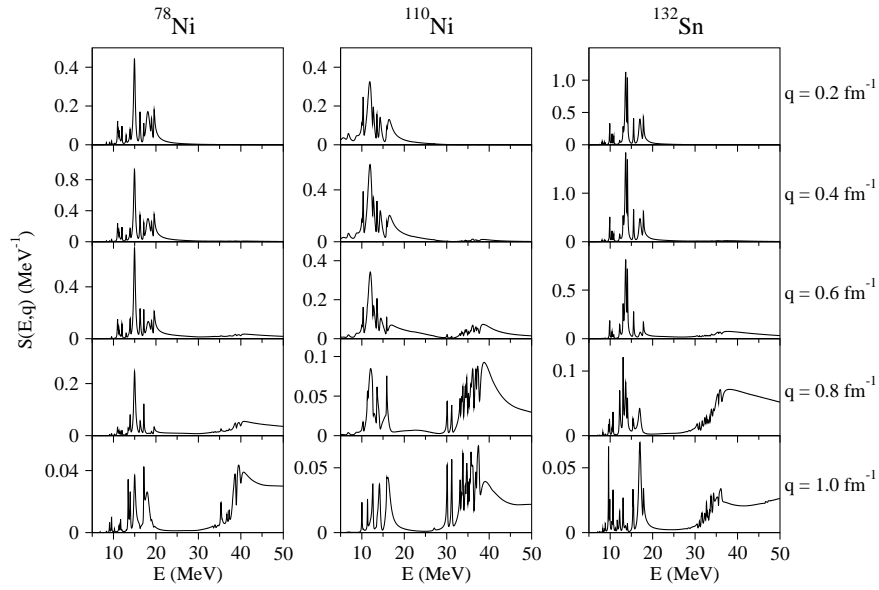


Figure 4: IVD strength distribution as a function of energy and momentum transfer.

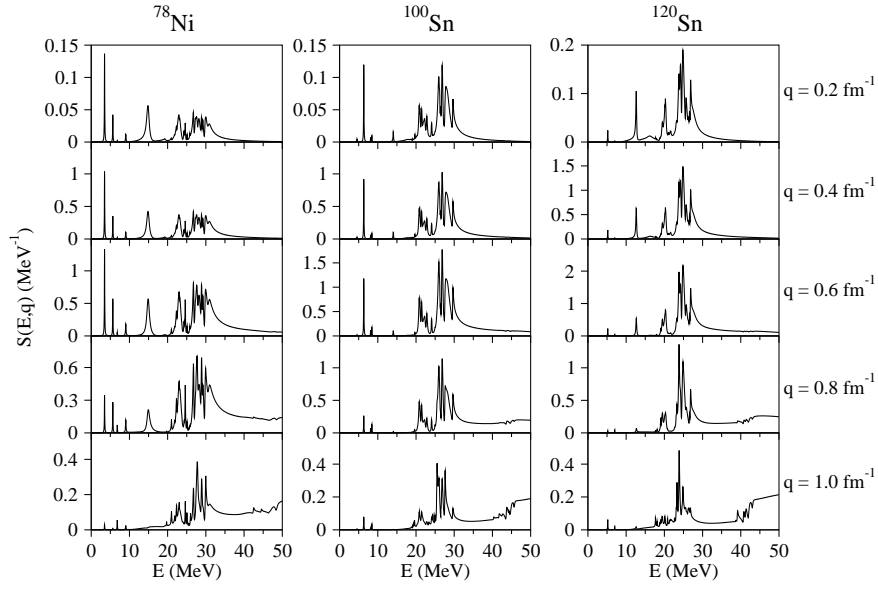


Figure 5: IVQ strength distribution as a function of energy and momentum transfer.

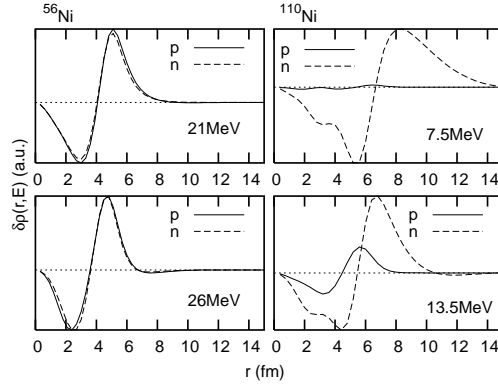


Figure 6: The transition density (in arbitrary units) for protons (full lines) and neutrons (dashed lines), corresponding to ISM transitions of the nuclei ^{56}Ni (left panel) and ^{110}Ni (right panel) at the indicated values of the energy.

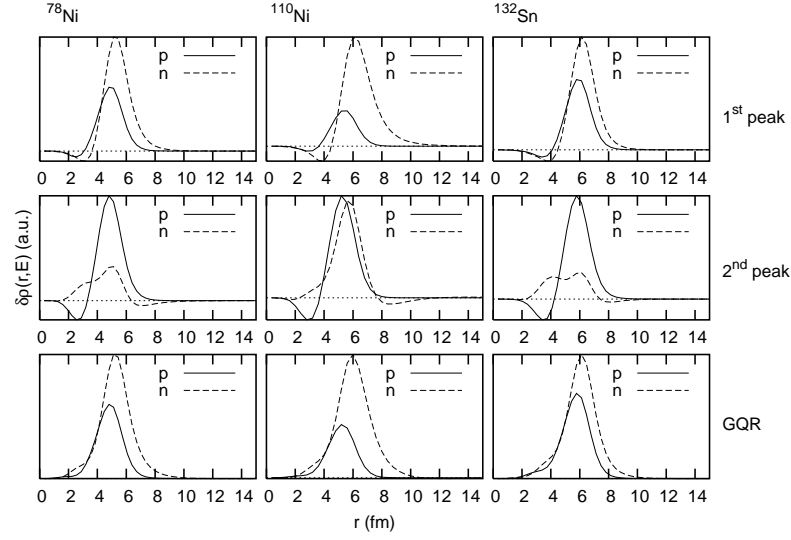


Figure 7: The transition density (in arbitrary units) for protons (full lines) and neutrons (dashed lines) corresponding to the first (collective) and second low-lying ISQ peaks and to the IS GQR, for the nuclei ^{78}Ni , ^{110}Ni and ^{132}Sn .

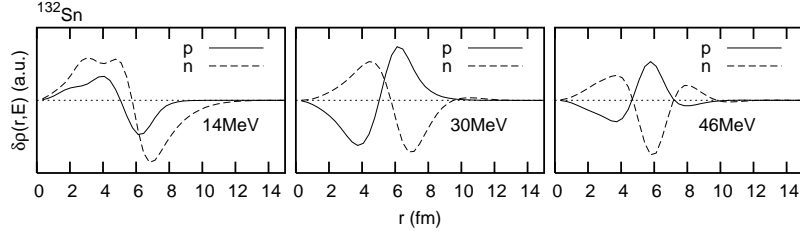


Figure 8: The transition density (in arbitrary units) for protons (full lines) and neutrons (dashed lines) corresponding to IVM transitions of the nucleus ^{132}Sn at the indicated values of the energy.

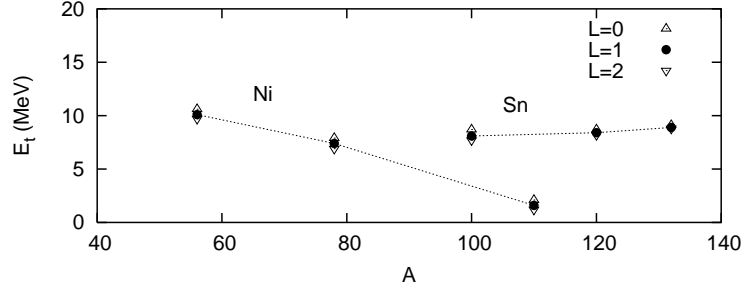


Figure 9: The calculated particle threshold energy E_t plotted vs the mass number A , for the isotopes $^{56,78,110}\text{Ni}$ and $^{100,120,132}\text{Sn}$ and for $L = 0, 1, 2$. Lines connecting isotopes of the same element are drawn to guide the eye.